International Journal of Chemical and Biochemical Sciences
(ISSN 2226-9614)

Journal Home page: www.iscientific.org/Journal.html

Microwave-assisted synthesis and characterization of $SrAl_2O_4$/Eu/Dy and the role of phosphorus dopants on its fluorescence and phosphorescence properties

*Seyed Mohsen Mousavi, *Shahram Moradi Dehaghi, Saeed Abedini Khorrami*

Department of Chemistry, North Tehran Branch, Islamic Azad University, Tehran, Iran

Abstract

The purpose of this study was the production of photoluminescent strontium aluminate phosphorous pigments using varied ratios of Sr, boric acid, Nd, and citric acid. These pigments are remarkably utilized in various areas. The presence of each one of these compounds has a significant impact on the fluorescence or phosphorescence effect, as well as their physical properties such as morphology and crystal structure. These physical changes were measured with spectroscopic methods. Some pigments had red emission under UV radiation before being subjected to the reduction process. After the reduction, they showed strong afterglow. 16 samples with different constituting components were prepared among which 8 were selected for this study, labeled samples S1 to S8. After the reduction process, they were labeled samples RS1 to RS8. The phosphorescence analysis with the wavelength of 254 and 360 nm demonstrated an intensity of 439 and 191 respectively for sample RS5, and 631 and 634 for the fluorescence measurement with the wavelength of 254 and 360 nm for the same sample. The sample RS5 demonstrated the longest afterglow of about 4 hours.

Keywords: Microwave synthesis, Phosphorescence, Fluorescence, Dopant Phosphors.

Full length article **Corresponding Author*, e-mail: shm_moradi@iau-tnb.ac.irb Doi # https://doi.org/10.62877/60-IJCBS-24-25-19-60

1. Introduction

One of the methods for saving energy in infrastructures and buildings where brightness is essential to remain for residents after the sunset, such as metro stations, roads, hospitals, or exits is employing materials with afterglow properties. Strontium aluminates are susceptible compounds with luminescence properties. If dopants such as Eu, Dy, Nd, or other compounds are doped into their crystal lattice during their production, they gain phosphorescence properties based on the amounts of dopants for an extended period. The afterglow property has been investigated in innumerable pieces of researches. Phosphors are materials that demonstrate the fluorescence or phosphorescence phenomenon. Phosphors owning fluorescence and phosphorescence properties were first manufactured in the 20th century. The mentioned phosphors were composed of ZnS which was doped with Mg and Cu. Cobalt was another dopant added to the mentioned composite as a co-dopant. Later, alkaline earth metals including Ca and Sr were employed instead of Zn and different dopants consisting of Eu^{3+} and Ce^{3+} were used. Strontium aluminates doped with europium are edge-cutting materials owning durable afterglows compared to the traditional ZnS compounds [1]. Strontium aluminates possess six common forms including $SrAl_{12}O_{19}$, $SrAl_4O_7$, $SrAl_2O_4$, $Sr_2Al_6O_{11}$, $Sr_3Al_2O_6$, and $Sr_4Al_{14}O_{25}$ [2-7]. $SrAl_2O_4$ is one of the most attention-grabbing compounds among them with excellent luminescence properties. $SrAl_2O_4$ doped with Eu was presented by Palilla et al. and it was announced that to possess a green afterglow with a maximum intensity at 520 nm. $SrAl_2O_4$: Eu^{2+}, Dy^{3+} as another groundbreaking compound was presented by Matsuzawa, declaring that the presence of Dy plays a crucial role in the afterglow effect [8]. The hole-electron mechanism was introduced as the explanation for the afterglow properties [8-16]. Production of $SrAl_2O_4$: Eu^{2+}, Dy^{3+}, Nd^{3+} via laser was reported by A. H. Wako et al. They mentioned the high photoluminescence properties of their synthesized compounds [17]. In 2007, Tadashi Ishigaki et al. reported successful synthesize of $SrAl_2O_4$: Eu^{2+}, Dy^{3+} employing carbon as a reductive agent. The process was performed in a microwave oven [18]. There are a variety of methods for the production of these luminescent compounds including solid-state reaction as the most employed method [8, 19-25], sol-gel [2, 7, 26-29], reverse micro-emulsion [30-33], and solution combustion synthesis (SCS) [34-37]. SCS is reported as one of the most trustworthy and feasible methods since it presents a small crystal size, is economic, and is quite safe. Tadashi et al. had precise investigations on

the results of the XRD and PL techniques for the samples before the reduction process and after that [18]. Rojas et al. reviewed $SrAl_2O_4$/Eu/Dy phosphors as the most studied material. They discussed different methods for synthesizing this material and the conditions they need along with the pros and cons of each method, the challenges for producing low-cost/temperature persistent nanostructures, the efficiency of each product, and their future applications [38]. Tang et al. evaluated $SrAl_2O_4$/Eu/Dy phosphors for potential applications in thermoluminescent dosimetry. It was proved that the mentioned phosphor demonstrates a linear response to both electron and photon beams, making it suitable to play the dosimeter role [39]. Zhilin et al. employed $SrAl_2O_4$/Eu/Dy phosphors to manufacture high-strength flexible films with long afterglow luminescent with introducing the mentioned phosphors into a TEMPO-oxidized nanofibrillated cellulose (ONFC) matrix [40]. Rojas et al. prepared a cost-efficient $SrAl_2O_4$/Eu/Dy film by a screen-printing method on a Al_2O_3 substrate. They used molten salt that generates a reactive ink-paste as a proper precursor for the film [41]. Atul et al studied the structural, thermal, vibrational and light emission feature of Dy, Eu, Sm, Er and Mn doped $SrAl_2O_4$ and CaAlO phosphors. they noticed that CaAlO phosphors have better thermal stability compared to $SrAl_2O_4$ phosphors [42]. The current study as a modified investigation of Tadashi et al. focused on the influence of the concentration of Sr, citric acid, Nd, and boric acid on photoluminescence properties of produced compounds in presence of Eu and Dy. This study was implemented after the previous one as an investigation on the role of dopants on $SrAl_2O_4$:Nd^{3+} composites produced in the microwave [43]. The novelty of our study is the employment of microwave as a facilitator for the first stage of producing the precursor phosphors, production of doped $SrAl_2O_4$ in presence of citric acid, Nd, boric acid and Dy altogether and separately in turns and reduction/calcination of each sample separately and studying the effect of presence of each material on different properties of the produced phosphors.

2. Experimental

2.1. Materials and methods

The employed materials in the study are as follows: purified water, $Eu(NO_3)_3{\cdot}6H_2O$ (99%), $Al(NO_3)_3.9H_2O$ (99 %), $Dy(NO_3)_2.5H_2O$ (99%), $Sr(NO_3)_2$ (99 %), urea (99.5%), $Nd(NO_3)_3.6H_2O$ (99%), anhydrous citric acid (99%), and Boric acid (99%), all purchased from Merck company. The initial materials proportions are brought in Table 1. Adequate water was poured over the initial materials in a small flask. After thorough mixing on a heater, a transparent viscous solution was produced. The solution was then poured into a crucible and was subjected to a microwave oven where the combustion reaction accomplished. The reaction duration was around 5 minutes. Then the resulting foamy and fragile products were gently pulverized and prepared for the upcoming analysis and processes. The samples were labelled S1, S2, S3, S4, S5, S6, S7, and S8. Then they were subjected to a reductive furnace placed on special boat crucibles. Pure hydrogen with atmospheric pressure was introduced to the furnace while the samples were undergoing the 1350 ºC of calcination temperature for an hour. The samples reduced in mass drastically because of the burning of extra nitrates. The decreased mass ratio was average 40%. The compounds after the reduction process were labelled samples RS1, RS2, RS3, RS4, RS5, RS6, RS7, and RS8. Table 1 demonstrates the initial mass ratio of the samples in grams before the microwave oven processing.

2.2. Instrumentation

Precursor samples were produced in the lab microwave LG 8265 1880 W. The luminescence spectroscopy was carried out employing a Perkin Elmer LS 55 fluorescence spectrometer at room temperature. XRD spectroscopy was done using the STOE STADI P, 40 kV, and 30 mA spectrometer with Cu lamps at room temperature. FTIR spectroscopy was implemented using Thermo Nicolet 8700 IR spectrometer at room temperature. SEM imaging was performed using the Zeiss FE-SEM model SIGMA VP SEM microscope at room temperature. These analyses were implemented on each sample before and after applying the reduction procedure. The reduction procedure was done in a pressure-controlled tube furnace as shown in figure 1.

3. Results and discussion

3.1. XRD result analysis

The produced samples involve a variety of phases, identified with XRD analysis. The following tables indicate the data including standard and observed 2θs attributed to the samples. The crystal sizes were computed using the Scherrer equation:

$$d_c = \frac{k\theta}{\beta cos\theta}$$

In this equation, λ is the wavelength of X-ray beams, k is the proportionality constant, β is the line broadening at half the maximum intensity (FWHM), and θ is the Bragg angle. The majority of the produced samples contain $SrAl_2O_4$ as the main ingredient. Hence, the total crystal size is roughly close to the $SrAl_2O_4$ phase crystal size. Figure 2 represents the XRD curves of sample S2 and RS2 as an example. The implemented process was the reduction of S2 to RS2. The hexagonal phase occurring in $SrAl_2O_4$ converts into the monoclinic phase due to the reduction process. The 2θ=28.38 and 2θ=29.92 peaks belonging to the monoclinic phase were drastically intensified after the reduction process. On the other hand, 2θ=19.76 peak referring to $Sr(NO_3)_2$ had a drastic decrease in the intensity after the reduction furnace, demonstrating the burning of extra nitrates. Other phases such as $Eu_2B_2O_5$ were formed in the samples after the furnace process in around 2θ=35, as the 1350 °C of temperature along with the reduction process alters some of the phases and compounds with the new ones.

Table 2 shows the analysis of detailed XRD spectroscopy of the samples. Table 3 represents the main phases of samples before and after the reduction process.

3. 2. Analysis of photoluminescence properties

3.2.1. Analysis of afterglow

For this part of the study, we used a LED light to stimulate the samples. The LED light was in white, owning an intensity of 24000 lux. The stimulation was performed for 30 seconds. The intensity and the duration of the afterglow were registered as shown in figure 3. Sample RS5 was found to own the most afterglow intensity as soon as the stimulation source was stopped. It also had the longest afterglow of 1 hour due to the higher absorbed energy. After that, sample RS3 possessed the longest afterglow, followed by samples RS8, RS7, RS6, RS2, and RS4. Figure 3 demonstrates the

afterglow curves of the samples. Figure 4 demonstrates the afterglow picture of sample RS5 as the best sample.

3.2.2. Analysis of phosphorescence and Fluorescence results

The laser beam excited the samples to obtain the emissions. In fluorescence mode, the emission was analyzed while the laser beam was radiating the samples. In phosphorescence mode, it was done as soon as the exciting beam was ceased. Only two out of 16 sample curves are brought in figure 5.

3.2.2.1. Sample analysis before the reduction process

3.2.2.1.1. Fluorescence emission analysis resulted from the 254 nm excitation beam

Considering this analysis, we can conclude that the curves are related to the lattice emission. At 254 nm of excitation, the lattice shows an emission due to the presence of some highly excitable band gaps. After taking a better look at this specific excitation and emission curve, we realize that this curve formed due to the emission lattice of aluminate. A proof for this claim is observed in sample S1 (without strontium) in which the first corner of the peak is omitted (sample S5 owns the mentioned corner as the most prominent sample). Also, another curve can be found in the wavelength of 631 nm which could be attributed to the defects occurring in the lattice. Keep in mind that europium can cause a peak around the same wavelengths. Plenty of defects in the lattice structure is very common in the SCS process. Also, defections are one of the main parameters for the development of inter-state states of energy. Dopants provide numerous states like that, causing a major alternation in electron transitions from the higher conductivity band to the lower valence band. Hence, other than the sample S1, other samples show deviations from the maximum intensity. Extra boric acid in sample S4 slightly increased the intensity. The S4 curve matches the S5 curve.

3.2.2.1.2. Fluorescence emission analysis resulted from the 360 nm excitation beam

As it is observed in the curve, the lower excitation energy applied with the 360 nm beams led to a low energy emission in comparison to the previous excitation beam (254 nm). The band gaps might be influenced by the excitation factors due to the precursor materials size which was in the nano-scale. For instance, samples S7 and S8 demonstrated non-identical feedbacks to the excitation beams. It can be inferred that the presence of citric acid as a chelate has had remarkable repercussion on the lattice. In general, the strontium aluminate lattice has generated the majority of the emission as a reaction to the low-energy excitation beam. Varying parameters significantly influence the crystallization degree and in other words, the lattice emission intensity. As proof to this claim, we can refer to sample S1 with the maximum emission intensity which lacks Sr. Sample S8 is purely strontium nitrate, therefore it possesses different emission spectra. However, in the case of sample S7, only an aluminate lattice is being observed which its nitrate can be amorphous. Therefore, due to the pureness of nitrates in sample S8, the least intensity belongs to it accordingly.

3.2.2.1.3. Phosphorescence emission analysis resulted from the 254 nm excitation beam

As figure 5 demonstrates, the phosphorescence curve is incompatible. The obtained curve intensity is nearly zero for all the samples. This can be attributed to the competition between the development of inter-states of phosphorescence and defections. Hence, any small fluctuation in the sample composition leads to much lower emission intensities. Sample S5 owned the highest emission intensity followed by samples S3 and S6. Extra boric acid in sample S4 slightly reduced the intensity in comparison to sample S3 with no boric acid content.

3.2.2.1.4. Phosphorescence emission analysis resulted from the 360 nm excitation beam

Unlike the previous phosphorescence curve, this curve seems to possess the right excitations beam which is the low-energy excitation beam. Phosphorescence is obtained with low energy excitation. There are three identical regions in this curve. Sample S5 owns the most emission intensity. It can be inferred that the absence of Nd boosts the emission. Probably Nd can act as a competitor and the charge transfer to its states decreases the emission intensity. Sample S5 owned the highest emission intensity followed by samples S3 and S6. Extra boric acid in sample S4 marginally reduced the intensity in comparison to sample S3 with no boric acid content.

3.2.2.2. Sample analysis after the reduction process

3.2.2.2.1. Fluorescence emission analysis resulted from the 254 nm excitation beam

As the curves demonstrate, the reduction process thoroughly modified the curve appearance. This is due to the fluorescence-phosphorescence competition. The reduction process reduced the Eu^{3+} centers to Eu^{2+}. This promotes the $4f^6$ to $5d^7$ electron transfers which are responsible for the phosphorescence emission at 520 nm. Hence, the phosphorescence effect was observed more than fluorescence. The disappearance of the peak at 610 nm is because of the mentioned reduction in Eu. The peaks belonging to Eu^{3+} can be observed with a 254 nm excitation beam. The observed increased intensities in these curves compared to the ones before reduction has a root in the high crystallinity of the current samples after the reduction/heat process. Sample RS5 owns the highest fluorescent emission followed by sample RS3 and RS7.

3.2.2.2.2. Fluorescence emission analysis resulted from the 360 nm excitation beam

The curves here have high similarities to the previously analyzed ones. Of course, there are small divergences between them such as the peak position. Drastic changes in the lattice due to the reduction/heat process are the origin of this similarity between the 254 and 360 nm emission curves. Also except for the sample RS5 with no Nd, other samples underwent blueshifts. The presence of Nd ions influences the crystal structure and shift the peak from 514 nm to 503 nm. Sample RS5 possesses the highest fluorescent emission followed by sample RS3 and RS7.

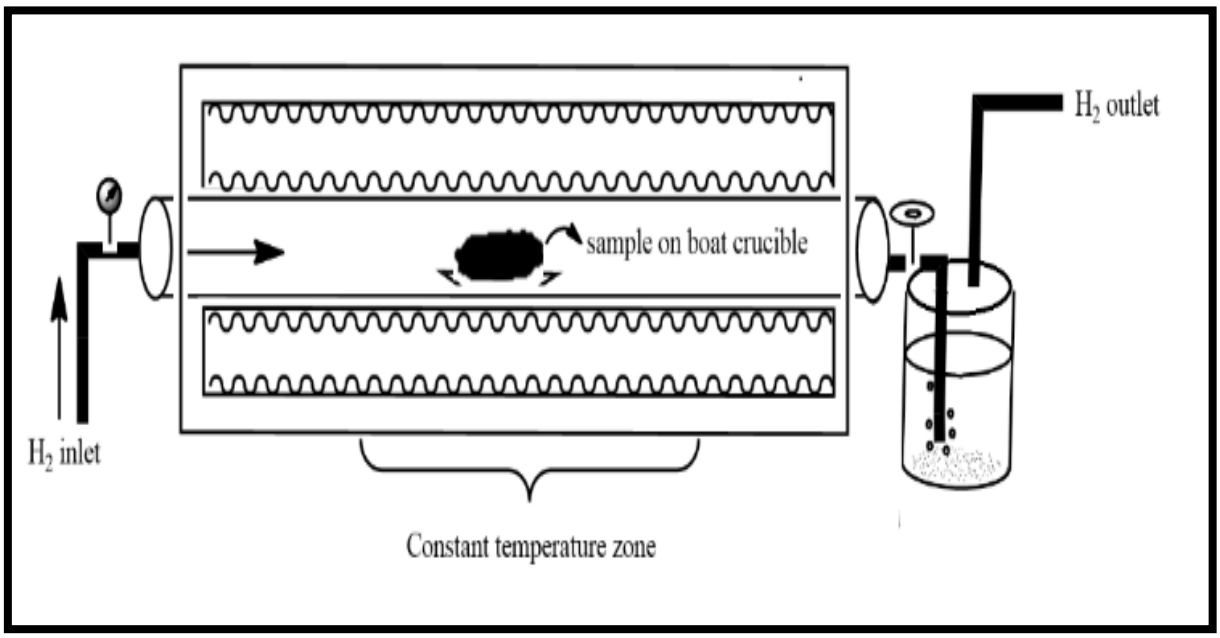

Figure 1: Schematic figure of the tube furnace

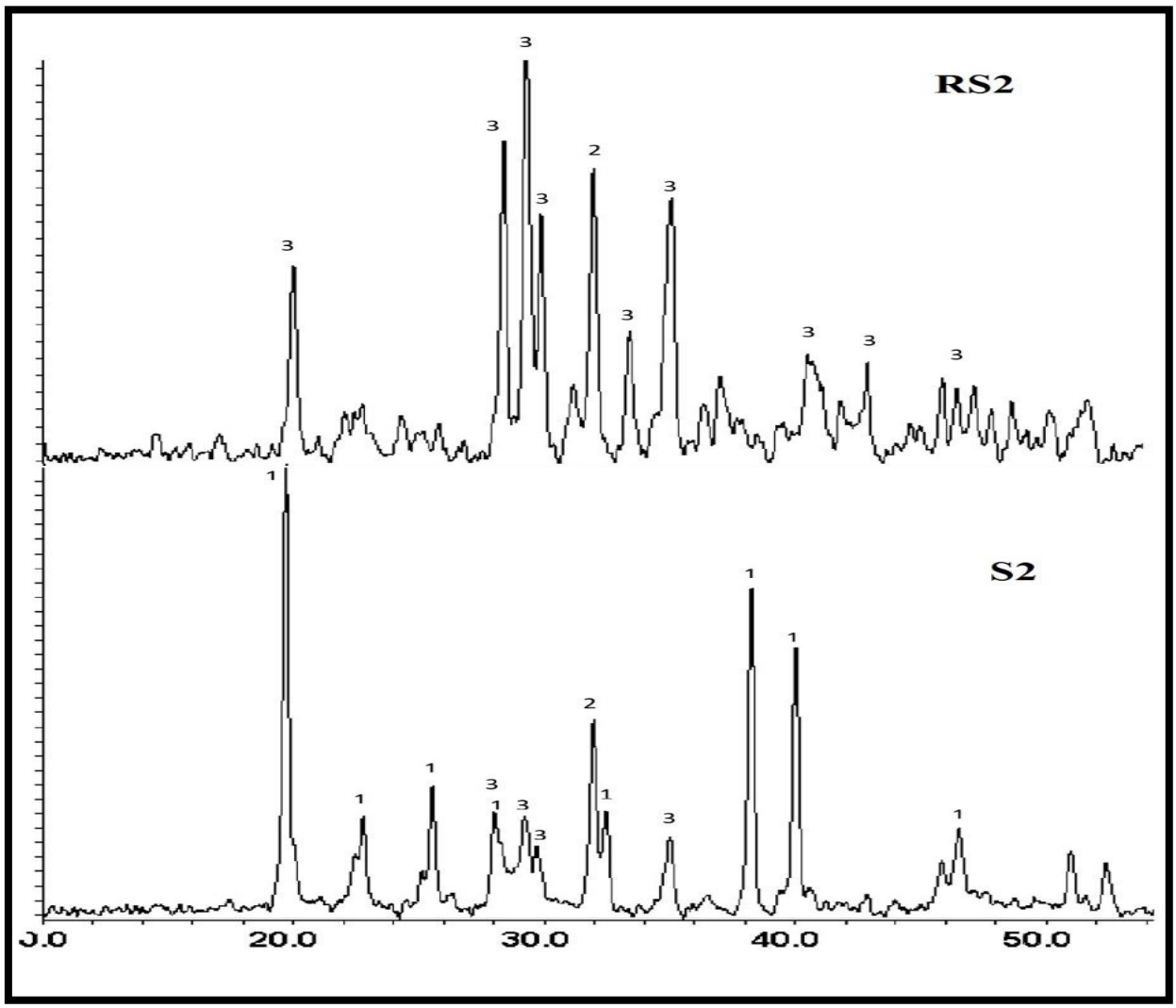

Figure 2: XRD analysis of sample S2 and RS2 where 1 represents $Sr(NO_3)_2$, 2 represents $Sr_3Al_2O_6$, and 3 represents $SrAl_2O_4$

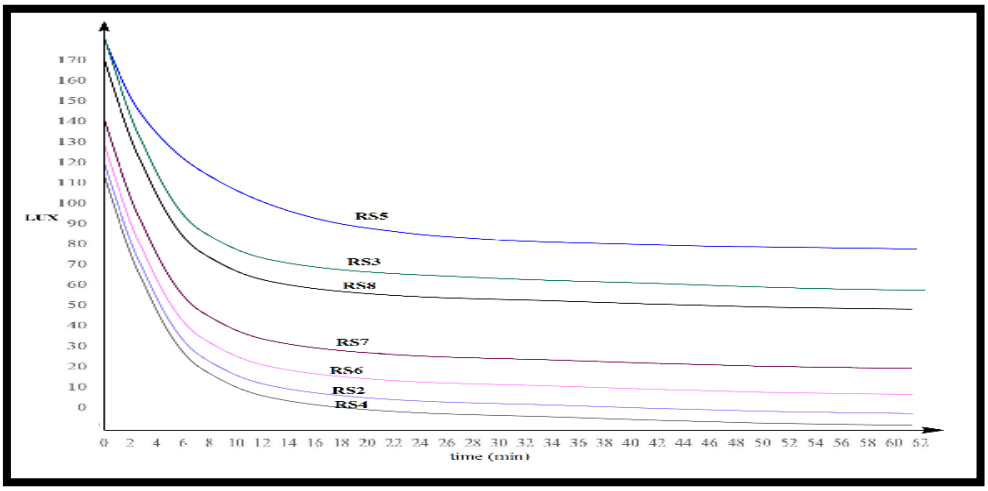

Figure 3: Afterglow decay curves of samples with afterglow properties

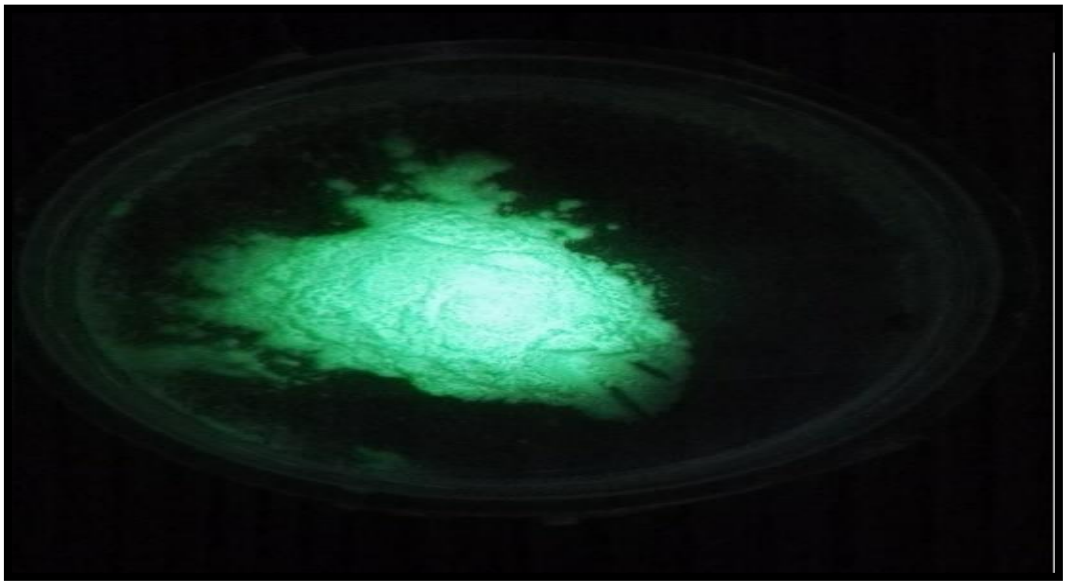

Figure 4: Afterglow illustration of sample RS5

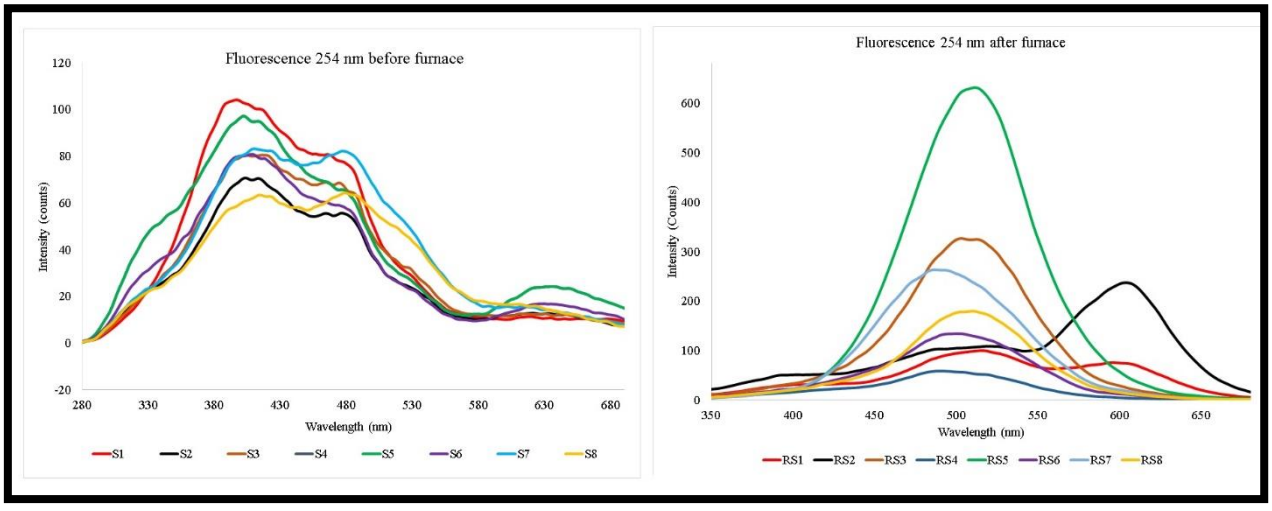

Figure 5: Photoluminescence results of samples S1-S8 (before furnace/reduction) and RS1-RS8 (after furnace/reduction).

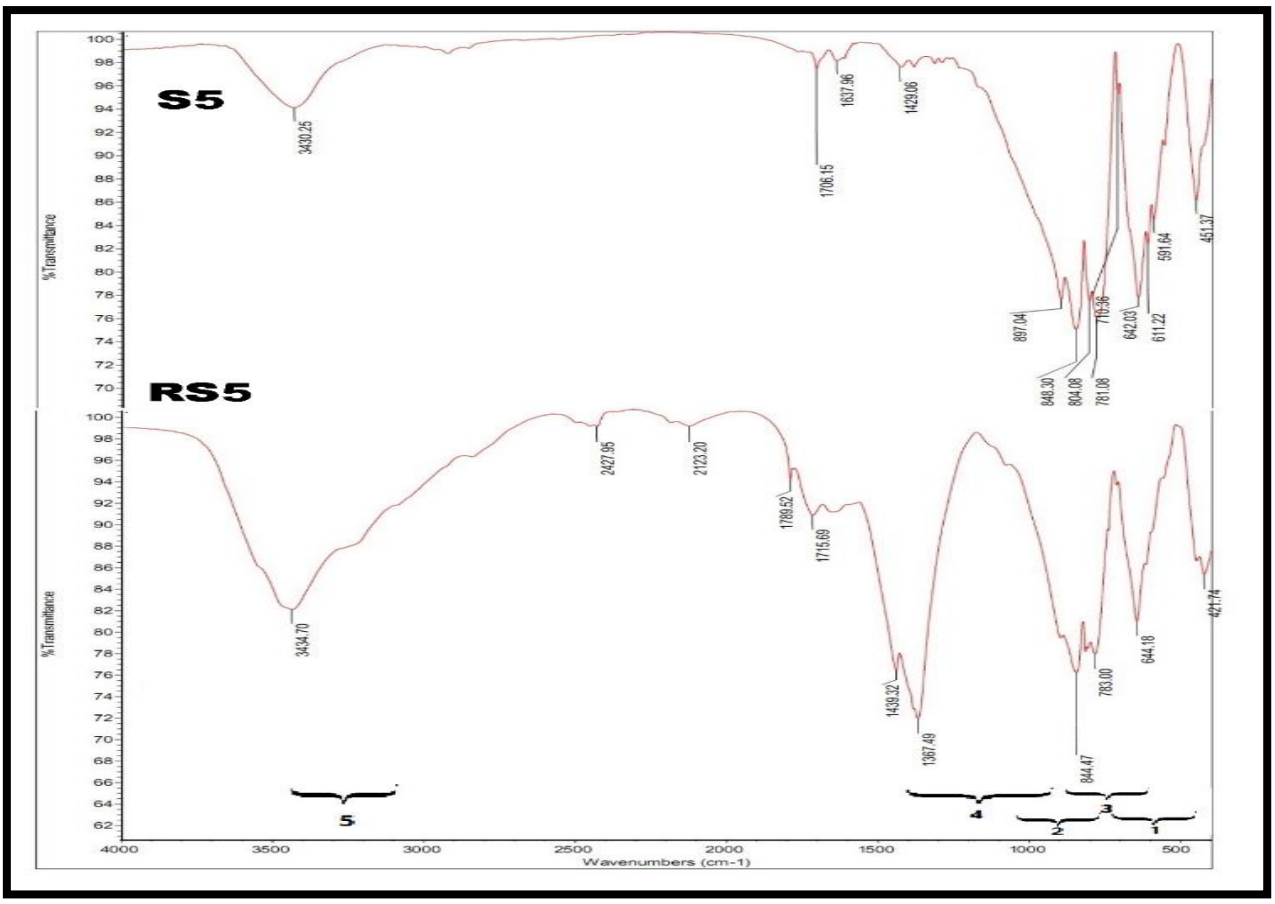

Figure 6: IR analysis of samples S5 and RS5 where 1 is the antisymmetric bending of O-Al-O, 2 is antisymmetric stretching of Al-O-Al, 3 is symmetric stretching of O-Al-O, 4 is vibrational stretching of BO_3 and BO_4, and 5 is stretching of OH groups.

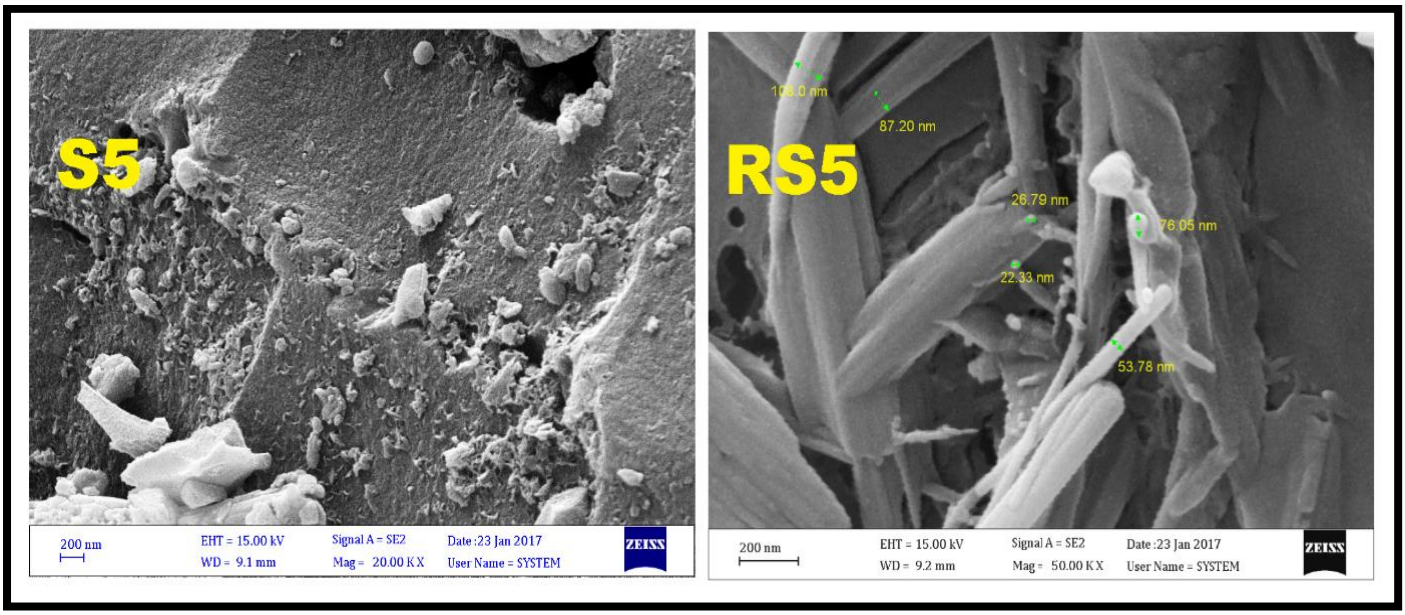

Figure 7: SEM analysis of samples S5 and RS5

Table 1: Mass ratios of precursor samples (g)

Samples	$Eu(NO_3)_3.6H_2O$	$Dy(NO_3)_3.6H_2O$	$Sr(NO_3)_2$	H_3BO_3	Citric acid	Urea	$Nd(NO_3)_3.6H_2O$	$Al(NO_3)_3.9H_2O$
S1	0.02	0.04	0	0.06	0	4	0.02	3.74
S2	0.02	0.04	2	0.06	0	4	0.02	3.74
S3	0.02	0.04	1	0	0	4	0.02	3.74
S4	0.02	0.04	1	0.12	0	4	0.02	3.74
S5	0.02	0.04	1	0.06	0	4	0	3.74
S6	0.02	0.04	1	0.06	0	4	0.04	3.74
S7	0.02	0.04	1	0.06	0.03	4	0.02	3.74
S8	0.02	0.04	1	0.06	0.06	4	0.02	3.74

Table 2: Analysis of detailed XRD spectroscopy of the samples

Sample number	Phases	Observed 2θ angle	Observed intensity	hkl	Standard 2θ angle	Standard intensity	Crystal size(nm)
S1	$(NO)_2Al_{22}O_{34}$	7.66	100	002	7.818	100	37.66
		15.57	35.84	004	15.64	25	
		19.98	8.15	102	19.93	30	
		31.91	35.21	107	31.19	40	
		35.65	40.30	114	35.74	35	
		44.36	9.12	206	44.34	25	
		66.66	48.79	220	66.76	45	
	Dy_2O_3	29.36	29.98	110	29.65	100	52.99
RS1	$EuAlO_3$	23.81	9.17	002	23.836	80.0	59.06
		33.95	22.03	112	33.94	100	
		48.68	7.21	004	48.79	60	
	Al_2O_3	25.54	52.92	012	25.54	67.8	45.60
		35.13	92.46	104	35.10	100	
		37.65	33.61	110	37.7	45	
		43.28	100	113	43.30	96	
		57.36	90.36	116	57.42	90.9	
		68.06	43.53	300	68.12	53.2	
	$SrAl_2O_4$	29.17	19.63	220	29.27	91	72.71
		34.98	15.74	031	35.11	69	
	$Sr(NO_3)_3$	19.71	100	111	19.64	100	

		25.51	27.63	210	25.44	24.9	
S2		32.45	21.54	220	32.34	21.4	40.91
		38.27	67.89	311	38.12	71.6	
		39.97	57.14	222	39.89	55.9	
		31.93	41.63	440	31.94	100	41.93
	$Sr_3Al_2O_6$	45.79	10.23	800	45.76	30	
	$SrAl_2O_4$	20	48.12	011	19.94	49.70	
		22.74	13.95	120	22.74	18.7	
		29.22	100	220	29.29	94.2	38.83
		35.12	54.47	031	35.12	72.1	
		42.86	21.82	400	42.86	19.5	
RS2		47.13	15.7	222	47.12	22.9	
	$Sr_3Al_2O_6$	31.90	70.63	440	31.90	100	48.79
	$Eu_2B_2O_5$	26.78	4	-202	26.76	30	72.34
	$SrAl_2O_4$	29.23	77.86	220	29.27	91	52.97
		34.98	15.74	031	35.11	69	
S3		19.72	100	111	19.64	100	
		25.53	25.36	210	25.44	24.9	
	$Sr(NO_3)_3$	32.49	18.53	220	32.34	21.4	47.62
		38.21	58.74	311	38.12	71.6	
		40.03	47.87	222	39.89	55.9	
		19.98	59.45	011	19.94	49.70	
		22.70	23.42	120	22.74	18.7	
	$SrAl_2O_4$	29.23	100	220	29.29	94.2	65.01
		35.03	81.13	031	35.12	72.1	
RS3		42.83	23.55	400	42.86	19.5	
		47.97	21.59	222	47.12	22.9	
	Dy_2O_3	30.76	12.23	101	30.73	100	58.59
		19.76	100	111	19.64	100	
		25.59	30.38	210	25.44	24.9	
S4	$Sr(NO_3)_3$	32.41	24.07	220	32.34	21.4	38.14
		38.29	84.14	311	38.12	71.6	
		40.08	62.38	222	39.89	55.9	
		20.04	52.60	011	19.94	49.70	
		22.71	23.06	120	22.74	18.7	
		29.31	93.74	220	29.29	94.2	
	$SrAl_2O_4$	28.44	100	-211	28.38	100	58
RS4		35.13	82.83	031	35.12	72.1	
		42.91	26.10	400	42.86	19.5	

		47.24	28.97	222	47.12	22.9	
	Eu_2O_3	30.63	40.12	101	30.53	100	72
	$SrAl_2O_4$	29.30	28.64	220	29.27	91	
		35.10	18.28	031	35.11	69	58
S5		19.77	100	111	19.64	100	
		25.55	27.78	210	25.44	24.9	
	$Sr(NO_3)_3$	32.44	16.87	220	32.34	21.4	47
		38.30	70.50	311	38.12	71.6	
		40.15	54.58	222	39.89	55.9	
		20.08	52.84	011	19.94	49.70	
		22.65	17.07	120	22.74	18.7	
		28.38	100	-211	28.38	100	
	$SrAl_2O_4$	29.29	97.77	220	29.29	94.2	41
RS5		35.08	76.75	031	35.12	72.1	
		42.88	28.92	400	42.86	19.5	
		47.17	28.27	222	47.12	22.9	
	Eu_2O_3	30.54	8.20	101	30.53	100	72
	$SrAl_2O_4$	19.93	69.55	011	19.94	49.70	
		22.57	27.03	120	22.74	18.7	
		28.35	58.54	-211	28.38	100	
		29.13	100	220	29.29	94.2	71
		34.83	79.24	031	35.12	72.1	
		42.62	15.71	400	42.86	19.5	
S6		47.46	8.37	222	47.12	22.9	
		19.62	61.16	111	19.64	100	
		25.37	14.46	210	25.44	24.9	
	$Sr(NO_3)_3$	32.39	10.76	220	32.34	21.4	95
		38.15	38.81	311	38.12	71.6	
		39.86	29.83	222	39.89	55.9	
		19.97	51.15	011	19.94	49.70	
		22.77	20.45	120	22.74	18.7	
		28.44	91.05	-211	28.38	100	
	$SrAl_2O_4$	29.30	100	220	29.29	94.2	65
		35.16	68.58	031	35.12	72.1	
RS6		42.89	30.33	400	42.86	19.5	
		47.12	23.03	222	47.12	22.9	
	$NdAlO_3$	23.78	6.28	012	23.70	100	36
		33.86	19.66	104	33.87	97.7	
	B_2O_3	31.20	11.49	111	31.22	100	98

		20.00	64.52	011	19.94	49.70	
		22.63	20.89	120	22.74	18.7	
S7		28.37	76.32	-211	28.38	100	
		29.24	100	220	29.29	94.2	33
	$SrAl_2O_4$	34.95	80.04	031	35.12	72.1	
		42.80	21.13	400	42.86	19.5	
		47.15	20.62	222	47.12	22.9	
		20.00	55.86	011	19.94	49.70	
		22.66	18.86	120	22.74	18.7	
		28.45	80.59	-211	28.38	100	
	$SrAl_2O_4$	29.25	100	220	29.29	94.2	63
		35.12	77.69	031	35.12	72.1	
RS7		42.86	23.23	400	42.86	19.5	
		47.13	26.66	222	47.12	22.9	
	$SrAl_4O_7$	23.04	12.21	012	23.70	100	71
	Eu_2O_3	30.53	6.47	101	30.53	100	58
	NdO_2	27.92	12.26	111	27.87	100	97
		32.17	6.65	200	32.28	37	
		19.72	100	111	19.64	100	
		25.51	30.43	210	25.44	24.9	
S8	$Sr(NO_3)_3$	32.42	21.79	220	32.34	21.4	47
		38.26	68.42	311	38.12	71.6	
		40.00	60.56	222	39.89	55.9	
		20.04	47.33	011	19.94	49.70	
		22.68	20.32	120	22.74	18.7	
		28.39	96.04	-211	28.38	100	
RS8	$SrAl_2O_4$	29.22	100	220	29.29	94.2	36
		35.13	66.95	031	35.12	72.1	
		42.78	21.33	400	42.86	19.5	
		47.09	39.14	222	47.12	22.9	
	$SrAl_4O_7$	23.53	7.67	012	23.70	100	71

Table 3: Main phases of samples before and after the reduction process

Samples	Constituting Phases			
S1	$(NO)_2Al_{22}O_{34}$	Dy_2O_3		
S2	$SrAl_2O_4$	$Sr_3Al_2O_6$	$Eu_2B_2O_5$	
S3	$SrAl_2O_4$	$Sr(NO_3)_3$		
S4	$Sr(NO_3)_3$	$Sr(NO_3)_3$		
S5	$SrAl_2O_4$	$Sr(NO_3)_3$		
S6	$SrAl_2O_4$	$Sr(NO_3)_3$		
S7	$SrAl_2O_4$			
S8	$Sr(NO_3)_3$			
RS1	$EuAlO_3$	Al_2O_3		
RS2	$SrAl_2O_4$	$Sr_3Al_2O_6$	$Eu_2B_2O_5$	
RS3	$SrAl_2O_4$	Dy_2O_3		
RS4	$SrAl_2O_4$	Eu_2O_3		
RS5	$SrAl_2O_4$	Eu_2O_3		
RS6	$SrAl_2O_4$	$NdAlO_3$	B_2O_3	
RS7	$SrAl_2O_4$	$SrAl_4O_7$	Eu_2O_3	NdO_2
RS8	$SrAl_2O_4$	$SrAl_4O_7$		

Table 4:EDX mass analysis of precursor and final products

	wt% of elements							
Samples	B	Sr	O	C	Al	Eu	Dy	Nd
S1	16.4	18.1	12.3	33.6	16.6	1.3	1.1	0.6
RS1	15.8	19.9	34	12	16.2	0.5	0.8	0.8
S2	16.1	17.5	19	28.7	17.4	0.3	0.6	0.4
RS2	15.4	19.4	25	20.9	17.2	0.7	1.2	0.2
S3	15.4	19.9	12.5	33.5	16.3	0.3	1.4	0.7
RS3	16.7	19.3	25.3	19.2	17	0.6	1.3	0.6
S4	16.6	19	34.7	10.5	17.1	1.1	0.3	0.7
RS4	16.2	19.1	30.2	15	17.4	0.6	0.6	0.9
S5	16	19.5	32.9	11.9	17.9	0.5	0.9	0.4
RS5	16.9	18.8	17.5	28.5	16.8	0.6	0.4	0.5
S6	15.7	19.6	19.4	26.3	16	0.9	1.4	0.7
RS6	16.5	18.1	43	3.8	16	0.8	0.9	0.9
S7	15.1	19.3	34.3	13.4	16.2	0.9	0.5	0.3
RS7	16.4	18.4	20.1	24.8	17.6	0.6	1.3	0.8
S8	16.6	18.5	31.6	15.3	16.5	0.2	0.7	0.6
RS8	16.3	19.6	26.2	19.4	17.4	0.3	0.4	0.4

3.2.2.2.3. Phosphorescence emission analysis resulted from the 254 nm excitation beam

As the curves demonstrate, the majority of the samples manifested a phosphorescence effect after the reduction/heat process. We already admit that the 514 nm peak belongs to the Eu^{2+} centers. Another point is the sample RS2 which seems to be different due to the formation of competitor strontium aluminates. The red peak observed in this sample has a root in the structural deficiencies resulting from non-stoichiometric conditions of strontium aluminates. Sample RS5 possesses the highest fluorescent emission followed by sample RS3 and RS8.

3.2.2.2.4. Phosphorescence emission analysis resulted from the 360 nm excitation beam

This mode demonstrated the best phosphorescence effect. The position of the peak is fairly the same as the previous phosphorescence mode which was 513 nm. The best sample was sample RS5. A high phosphorescence effect emanates from an excellent composition balance. Extra boric acid in sample S4 reduced the intensity in comparison to the sample S3 with no boric acid content in all the curves after the heat/reduction process. Figure 5 demonstrates the phosphorescence and fluorescence curves of the samples before and after the heat/reduction process under 254 nm of excitation radiation. Generally, it can be inferred from the figure that the majority of the samples after the reduction process had fluorescence emission at 520 nm green spectrum which takes place due to the electron transition of $4f^65d$ to $4f^7$ in Eu^{2+} dopants. The same results have been obtained from other studies [7-12, 15, 17, 30] discussing the $SrAl_2O_4$: Eu^{2+}, Dy^{3+} emission results. Generally, the intensities of the curve peaks are different for the majority of the samples, while the peak wavelengths are fairly similar. The wavelength similarities match the constitution of the samples and their similarity, while the intensity differences match the concentration difference in the samples. Sample RS5 owns

the highest fluorescent emission followed by sample RS3 and RS8.

3.3. IR analysis

Antisymmetric stretching and bending are demonstrated in figure 6. The stretching curve of metal oxides at 3430 cm^{-1} had a drastic drop in the samples after the reductive/heat process. Also, it was concluded that the results obtained from the FT-IR spectroscopy were significantly similar. However, the reduction/heat process caused a significant change in the curve shape through the samples and there are obvious differences between the results before and after the process. The symmetric bending of O-Al-O at 420-447 cm^{-1}, the symmetric stretching of O-Al-O at 700 cm^{-1}, the anti-symmetric stretching of O-Al-O at 780-900 cm^{-1}, the anti-symmetric bending of O-Al-O at 550-650 cm^{-1}, and the stretching vibration of B-O at 850-1200 cm^{-1} as well as the OH stretching at 3500 cm^{-1}, symmetric vibration of $Sr(NO_3)_3$ at 1382 cm^{-1} and vibrational stretching of BO_3 and BO_4 are observed in figure 6.

3.4. SEM analysis

The SEM results obtained from a couple of the samples before and after the heat/reduction process is demonstrated in figure 7. As it is shown, the process imposed a drastic modification in the structure of the sample. The sample before the process had grainy accumulated structures which turned to stacked layers after the reduction/heat process. The average thickness of the layers was about 70 nm. Doubling $Sr(NO_3)_3$ from samples S1 to S2 had an increasing crystal size effect. Samples S3 and S7 resemble together as they have formed crustily layered and round particles after microwave procedure. Sample S8 owns big crystals which can be attributed to the presence of extra citric acid which increases the in-spot temperature and more agglomeration and increased particle size.

3.5. EDX results

Table 4 demonstrates the EDX results obtained from the samples. The EDX elemental analysis matches the initial compounds used in the study.

4. Conclusion

The calcinated doped $SrAl_2O_4$ pigments were studied with different techniques including photoluminescence, XRD, EDX, FT-IR, and SEM. The diversified initial substances include $Sr(NO_3)_2$, H_3BO_3, citric acid, and $Nd(NO_3)_3.6H_2O$. On the one hand, employing microwave synthesis set forth a bunch of supremacies, such as being time and energy-saving and being cost-effective. One of the superiorities of microwave synthesis was the very quick production of the precursor pigments, owning prominent fluorescence properties. They possessed unique phosphorescence properties after undergoing the reduction furnace stage. On the other hand, this method produced only fluorescence-active pigments in the first step, which even though they were interestingly UV-active, but had to be submitted to the reduction process to acquire further phosphorescence properties. Supplementary research for evaluating other possible methods combined with different reductive agents is suggested to discover the most optimum synthesis route.

5. Acknowledgment

Hereby, the authors would like to appreciate all the financial support and facilities provided by the Islamic Azad University, North Tehran Branch.

References

[1] Z. Fu, S. Zhou, T. Pan, S. Zhang. (2005). Band structure calculations on the monoclinic bulk and nano-SrAl2O4 crystals. Journal of Solid-State Chemistry. 178(1): 230-233.

[2] M. Elsagh, M. Rajabi, E. Amini. (2014). Characterization of SrAl 2 O 4: Eu 2+, Dy 3+ phosphor nano-powders produced by microwave synthesis route. Journal of Materials Science: Materials in Electronics. 25: 1612-1619.

[3] K. Pavani, J.S. Kumar, T. Sasikala, B. Jamalaiah, H.J. Seo, L.R. Moorthy. (2011). Luminescent characteristics of Dy3+ doped strontium magnesium aluminate phosphor for white LEDs. Materials Chemistry and Physics. 129(1-2): 292-295.

[4] S.H. Han, Y.J. Kim. (2006). Luminescent properties of Ce and Eu doped Sr4Al14O25 phosphors. Optical Materials. 28(6-7): 626-630.

[5] H.N. Luitel, T. Watari, R. Chand, T. Torikai, M. Yada. (2012). Photoluminescence properties of a novel orange red emitting Sr4Al14O25: Sm3+ phosphor and PL enhancement by Bi3+ co-doping. Optical Materials. 34(8): 1375-1380.

[6] F. An, J. Bai, A. Balantekin, H. Band, D. Beavis, W. Beriguete, M. Bishai, S. Blyth, K. Boddy, R. Brown. (2012). Observation of electron-antineutrino disappearance at Daya Bay. Physical Review Letters. 108(17): 171803.

[7] T. Peng, L. Huajun, H. Yang, C. Yan. (2004). Synthesis of SrAl2O4: Eu, Dy phosphor nanometer powders by sol–gel processes and its optical properties. Materials Chemistry and Physics. 85(1): 68-72.

[8] T. Matsuzawa, Y. Aoki, N. Takeuchi, Y. Murayama. (1996). A new long phosphorescent phosphor with high brightness, SrAl2 O 4: Eu2+, Dy3+. Journal of the Electrochemical Society. 143(8): 2670.

[9] M. Segall, P.J. Lindan, M.a. Probert, C.J. Pickard, P.J. Hasnip, S. Clark, M. Payne. (2002). First-principles simulation: ideas, illustrations and the CASTEP code. Journal of Physics: Condensed Matter. 14(11): 2717.

[10] E. Nakazawa, Y. Murazaki, S. Saito. (2006). Mechanism of the persistent phosphorescence in Sr4Al14O25: Eu and SrAl2O4: Eu codoped with rare earth ions. Journal of Applied Physics. 100(11): 1-10.

[11] T. Aitasalo, J. Hölsä, H. Jungner, M. Lastusaari, J. Niittykoski. (2002). Sol–gel processed Eu2+-doped alkaline earth aluminates. Journal of Alloys and Compounds. 341(1-2): 76-78.

[12] Y. Lin, Z. Zhang, F. Zhang, Z. Tang, Q. Chen. (2000). Preparation of the ultrafine SrAl2O4: Eu, Dy needle-like phosphor and its optical properties. Materials Chemistry and Physics. 65(1): 103-106.

[13] A.J. Lenus, K.G. Rajan, M. Yousuf, D. Sornadurai, B. Purniah. (2002). Luminescence behaviour of rare

earth doped alkaline earth aluminates prepared by the halide route. Materials Letters. 54(1): 70-74.

[14] C. Chang, D. Mao. (2004). Long lasting phosphorescence of Sr4Al14O25: Eu2+, Dy3+ thin films by magnetron sputtering. Thin solid films. 460(1-2): 48-52.

[15] S. Tanabe, T. Hanada, M. Watanabe, T. Hayashi, N. Soga. (1995). Optical Properties of Dysprosium-Doped Low-Phonon-Energy Glasses for a Potential 1.3 μm Optical Amplifier. Journal of the American Ceramic Society. 78(11): 2917-2922.

[16] W. Jia, H. Yuan, L. Lu, H. Liu, W. Yen. (1998). Phosphorescent dynamics in SrAl2O4: Eu2+, Dy3+ single crystal fibers. Journal of Luminescence. 76: 424-428.

[17] A.H. Wako, F. Dejene, H. Swart. (2016). Structural and luminescence properties of SrAl2O4: Eu2+, Dy3+, Nd3+ phosphor thin films grown by pulsed laser deposition. Physica B: Condensed Matter. 480: 116-124.

[18] T. Ishigaki, H. Mizushina, K. Uematsu, N. Matsushita, M. Yoshimura, K. Toda, M. Sato. (2010). Microwave synthesis technique for long phosphorescence phosphor SrAl2O4: Eu2+, Dy3+ using carbon reduction. Materials Science and Engineering: B. 173(1-3): 109-112.

[19] H. Yamamoto, T. Matsuzawa. (1997). Mechanism of long phosphorescence of SrAl2O4: Eu2+, Dy3+ and CaAl2O4: Eu2+, Nd3+. Journal of Luminescence. 72: 287-289.

[20] T. Takeyama, T. Nakamura, N. Takahashi, M. Ohta. (2004). Electron paramagnetic resonance studies on the defects formed in the Dy (III)-doped SrAl2O4. Solid state sciences. 6(4): 345-348.

[21] F. Clabau, X. Rocquefelte, S. Jobic, P. Deniard, M.-H. Whangbo, A. Garcia, T. Le Mercier. (2005). Mechanism of phosphorescence appropriate for the long-lasting phosphors Eu2+-doped SrAl2O4 with codopants Dy3+ and B3+. Chemistry of Materials. 17(15): 3904-3912.

[22] F. Clabau, X. Rocquefelte, S. Jobic, P. Deniard, M.-H. Whangbo, A. Garcia, T. Le Mercier. (2007). On the phosphorescence mechanism in SrAl2O4: Eu2+ and its codoped derivatives. Solid state sciences. 9(7): 608-612.

[23] F. Clabau, X. Rocquefelte, T. Le Mercier, P. Deniard, S. Jobic, M.-H. Whangbo. (2006). Formulation of phosphorescence mechanisms in inorganic solids based on a new model of defect conglomeration. Chemistry of Materials. 18(14): 3212-3220.

[24] D. Haranath, V. Shanker, H. Chander, P. Sharma. (2003). Tuning of emission colours in strontium aluminate long persisting phosphor. Journal of Physics D: Applied Physics. 36(18): 2244.

[25] Y. Song, S. Choi, H. Moon, T. Kim, S.-I. Mho, H. Park. (1997). Phase studies of SrO Al2O3 by emission signatures of Eu2+ and Eu3+. Materials research bulletin. 32(3): 337-341.

[26] P. Escribano, M. Marchal, M.L. Sanjuán, P. Alonso-Gutiérrez, B. Julián, E. Cordoncillo. (2005). Low-temperature synthesis of SrAl2O4 by a modified sol–gel route: XRD and Raman characterization. Journal of Solid-State Chemistry. 178(6): 1978-1987.

[27] T.-P. Tang, C.-M. Lee, F.-C. Yen. (2006). The photoluminescence of SrAl2O4: Sm phosphors. Ceramics international. 32(6): 665-671.

[28] S. Wu, S. Zhang, J. Yang. (2007). Influence of microwave process on photoluminescence of europium-doped strontium aluminate phosphor prepared by a novel sol–gel-microwave process. Materials Chemistry and Physics. 102(1): 80-85.

[29] I.-C. Chen, T.-M. Chen. (2001). Sol-gel synthesis and the effect of boron addition on the phosphorescent properties of SrAl2O4: Eu2+, Dy3+ phosphors. Journal of Materials Research. 16(3): 644-651.

[30] J. Wang, L.S. Ee, S. Ng, C. Chew, L. Gan. (1997). Reduced crystallization temperature in a microemulsion-derived zirconia precursor. Materials Letters. 30(1): 119-124.

[31] J.H. Adair, E. Suvaci. (2000). Morphological control of particles. Current opinion in colloid & interface science. 5(1-2): 160-167.

[32] S. Vaidya, J. Ahmed, A.K. Ganguli. (2008). Controlled Synthesis of Nanomaterials using Reverse Micelles. Defence science journal. 58(4): 1-10.

[33] C.-H. Lu, S.-Y. Chen, C.-H. Hsu. (2007). Nanosized strontium aluminate phosphors prepared via a reverse microemulsion route. Materials Science and Engineering: B. 140(3): 218-221.

[34] T. Peng, H. Yang, X. Pu, B. Hu, Z. Jiang, C. Yan. (2004). Combustion synthesis and photoluminescence of SrAl2O4: Eu, Dy phosphor nanoparticles. Materials Letters. 58(3-4): 352-356.

[35] R. Zhang, G. Han, L. Zhang, B. Yang. (2009). Gel combustion synthesis and luminescence properties of nanoparticles of monoclinic SrAl2O4: Eu2+, Dy3+. Materials Chemistry and Physics. 113(1): 255-259.

[36] V. Singh, J.J. Zhu, V. Natarajan. (2006). Eu2+, Eu3+ and Sm3+ emission in SrAl12O19 phosphors prepared via combustion synthesis. physica status solidi (a). 203(8): 2058-2064.

[37] N.M. Son, N.N. (2009). Trac In Synthesis of SrAl2O4: Eu2+ Dy3+ phosphorescence nanosized powder by combustion method and its optical properties, Journal of Physics. *Conf. Ser*. 187 012017. DOI 10.1088/1742-6596/187/1/012017

[38] R.E. Rojas-Hernandez, F. Rubio-Marcos, M.Á. Rodriguez, J.F. Fernandez. (2018). Long lasting phosphors: SrAl2O4: Eu, Dy as the most studied material. Renewable and Sustainable Energy Reviews. 81: 2759-2770.

[39] X. Tang, E.D. Ehler, E. Brost, D.C. Mathew. (2021). Evaluation of SrAl2O4: Eu, Dy phosphor for potential applications in thermoluminescent dosimetry. Journal of Applied Clinical Medical Physics. 22(5): 191-197.

[40] L. Zhang, S. Lyu, Z. Chen, S. Wang. (2018). Fabrication flexible and luminescent nanofibrillated cellulose films with modified SrAl2O4: Eu, Dy phosphors via nanoscale silica and aminosilane. Nanomaterials. 8(5): 352-360.

[41] R.E. Rojas-Hernandez, F. Rubio-Marcos, A. Serrano, I. Hussainova, J.F. Fernandez. (2020). Boosting phosphorescence efficiency by crystal anisotropy in SrAl2O4: Eu, Dy textured ceramic layers. Journal of the European Ceramic Society. 40(4): 1677-1683.

[42] P. Kaur, A. Khanna. (2021). Structural, thermal and light emission properties of Eu, Sm, Dy, Er and Mn doped CaAl2O4 and SrAl2O4. Ceramics international. 47(10): 14655-14664.

[43] S.M. Mousavi, S.M. Dehaghi. (2019). Evaluation of Eu/Dy ratio on Nd-doped SrAl2O4 and their role on luminescence properties. Journal of Ceramic Processing Research. 20(3): 241-249.